J Geod (2006) 80: 47–60
DOI 10.1007/s00190-006-0029-9

ORIGINAL ARTICLE

A. Jäggi · U. Hugentobler · G. Beutler

Pseudo-stochastic orbit modeling techniques for low-Earth orbiters

Received: 1 March 2005 / Accepted: 24 January 2006 / Published online: 30 March 2006

Abstract The Earth's non-spherical mass distribution and atmospheric drag cause the strongest perturbations on very low-Earth orbiting satellites (LEOs). Models of gravitational and non-gravitational accelerations are utilized in dynamic precise orbit determination (POD) with GPS data, but it is also possible to derive LEO positions based on GPS precise point positioning without dynamical information. We use the reduced-dynamic technique for LEO POD, which combines the geometric strength of the GPS observations with the force models, and investigate the performance of different pseudo-stochastic orbit parametrizations, such as instantaneous velocity changes (pulses), piecewise constant accelerations, and continuous piecewise linear accelerations. The estimation of such empirical orbit parameters in a standard least-squares adjustment process of GPS observations, together with other relevant parameters, strives for the highest precision in the computation of LEO trajectories. We used the procedures for the CHAMP satellite and found that the orbits may be validated by means of independent SLR measurements at the level of 3.2 cm RMS. Validations with independent accelerometer data revealed correlations at the level of 95% in the along-track direction. As expected, the empirical parameters compensate to a certain extent for deficiencies in the dynamic models. We analyzed the capability of pseudo-stochastic parameters for deriving information about the mismodeled part of the force field and found evidence that the resulting orbits may be used to recover force field parameters, if the number of pseudo-stochastic parameters is large enough. Results based on simulations showed a significantly better performance of acceleration-based orbits for gravity field recovery than for pulse-based orbits, with a quality comparable to a direct estimation if unconstrained accelerations are set up every 30 s.

A. Jäggi (✉) · U. Hugentobler · G. Beutler
Astronomical Institute, University of Bern, Sidlerstrasse 5,
3012 Bern, Switzerland
E-mail: adrian.jaeggi@aiub.unibe.ch
Tel.: +41-31-6318592
Fax: +41-31-6313869

Keywords Low-Earth orbiter (LEO) · Precise orbit determination (POD) · Pseudo-stochastic orbit modeling · GPS

1 Introduction

Gravitational forces related to the Earth's oblateness and the non-gravitational forces due to residual atmospheric densities are responsible for the strongest perturbations acting on satellites in very low-Earth orbits. These forces produce large periodic variations in the orbit and a decay in the orbital height. Radial orbit differences caused by atmospheric drag after one day may reach 150 m for an initial height of 500 km (Beutler 2004) during normal solar activity. In addition, major perturbations induced by higher-order terms of the Earth's gravity field and minor perturbations induced by solar radiation pressure pose a challenge for precise orbit determination (POD) for low-Earth orbiters (LEOs).

The determination of precise orbits using space geodetic techniques, such as Satellite Laser Ranging (SLR), has opened a new era for LEO POD and related applications. It has been shown that geophysically relevant information such as geocenter variations or gravity field coefficients can be extracted by combining many years of observations to geodetic satellites (Reigber 1989). LEO POD is also a necessity for missions of Earth observing satellites, e.g., the determination of ocean topography from the TOPEX/Poseidon mission (Fu et al. 1994). This was the first extensive use of the Global Positioning System (GPS) with a spaceborne receiver for LEO POD (Bertiger et al. 1994). The geometric strength of continuously collected GPS observations allowed for orbit determination to closer than 3 cm in the radial direction. This mission stimulated a number of follow-up satellite missions to carry on-board GPS receivers for POD, but also for other purposes such as atmospheric sounding (e.g., Kursinski et al. 1997).

The launch of the CHAllenging Minisatellite Payload (CHAMP) on July 15, 2000, opened a new era in processing GPS data from spaceborne receivers. The combined analysis of non-conservative accelerations, which were

directly measured with unprecedented accuracy by an onboard accelerometer (Touboul et al. 1999), and the GPS tracking data proved the feasibility to separate gravitational from non-gravitational perturbations for gravity field estimation (Reigber et al. 2002). The large number of high quality global gravity field models underscores the success of CHAMP (e.g., Reigber et al. 2003, 2004). Current (GRACE) and future (GOCE) gravity field recovery missions, which aim to recover the gravity field with unprecedented accuracy, therefore pose the highest requirements on POD, e.g., 2 cm RMS in each direction for GOCE (ESA 1999).

There are many different studies for CHAMP POD based on GPS tracking data (e.g., Švehla and Rothacher 2002; van den IJssel et al. 2003; König et al. 2004). Most of them are based on a technique called "reduced-dynamic" (Wu et al. 1991), which exploits the geometric strength of the GPS observations to reduce the dependency on dynamic models (see Sects. 5 and 6). Due to CHAMP's very low altitude (below 450 km), it is common practice to solve for a large number of empirical parameters to compensate for deficiencies in the dynamic models. An alternative kinematic approach was successfully demonstrated for CHAMP by Švehla and Rothacher (2004), which yields precise ephemeris entirely by geometric means. Such positions are attractive mainly for gravity field estimation because they are independent of any dynamic models. Gerlach et al. (2003) used kinematic positions and accelerometer data and showed that gravity field models can be estimated with a quality comparable to the official CHAMP models by means of the energy integral method (O'Keefe 1957). The use of precise ephemeris for gravity field recovery had a considerably stimulating impact on several groups (e.g., Mayer-Gürr et al. 2004) due to less demanding computational resources as in the case of classical numerical integration techniques (e.g., Visser et al. 2003b).

In the following we consider pseudo-stochastic orbit modeling techniques for reduced-dynamic LEO POD as a powerful and efficient method to derive most precise satellite trajectories in the very low-Earth orbit (e.g., Visser and IJssel 2003a). Furthermore, we discuss different orbit representations and question whether such methodologies can be used to generate reduced-dynamic orbits, which could serve as input for a subsequent gravity field estimation process.

Section 2 reviews the methods of dynamic LEO POD. Section 3 presents two widely-used pseudo-stochastic orbit parametrizations and develops the mathematical background for a third, more refined orbit parametrization. CHAMP orbit results are shown in Sect. 4. Section 5 analyzes the presented methods in a more detailed way in a simulation environment and focuses, together with Sect. 6, on a possible use of reduced-dynamic orbits for gravity field estimation.

2 Dynamic orbit determination

The equation of motion of an Earth-orbiting satellite including all perturbations in the inertial frame reads as

$$\ddot{\mathbf{r}} = -GM\frac{\mathbf{r}}{r^3} + \mathbf{f}_1(t, \mathbf{r}, \dot{\mathbf{r}}, q_1, \ldots, q_d) \doteq \mathbf{f} \tag{1}$$

with initial conditions $\mathbf{r}^{(k)}(t_0) = \mathbf{r}^{(k)}(a, e, i, \Omega, \omega, T_0; t_0)$, $k = 0, 1$ (level of time differentiation). The parameters $a, e, i, \Omega, \omega, T_0$ are the six Keplerian elements pertaining to epoch t_0. $q_1, \ldots, q_d$ denote additional dynamical parameters considered as unknowns, e.g., scaling factors of analytically known accelerations, which describe deterministically the perturbing acceleration acting on the satellite.

Let us assume that an a priori orbit $\mathbf{r}_0(t)$ is available, e.g., from a GPS code solution. Dynamic orbit determination may then be considered as an orbit improvement process, i.e., the actual orbit $\mathbf{r}(t)$ is expressed as a truncated Taylor series with respect to the unknown orbit parameters p_i about the a priori orbit, which is represented by the parameter values p_{i0}:

$$\mathbf{r}(t) = \mathbf{r}_0(t) + \sum_{i=1}^{n} \frac{\partial \mathbf{r}_0(t)}{\partial p_i} \cdot (p_i - p_{i0}), \tag{2}$$

where $n = 6 + d$ denotes the total number of unknown orbit parameters, i.e., the six initial conditions for position and velocity and d dynamical parameters. Equation (2) allows us to improve the a priori orbit provided that the unknown orbit parameters and the partial derivatives of the a priori orbit with respect to those parameters are known.

2.1 Variational equations

Let us assume that p is one of the parameters defining the initial values or the dynamics in Eq. (1) and that the partial derivative of the a priori orbit $\mathbf{r}_0(t)$ with respect to the parameter p is designated by the function

$$\mathbf{z}_p(t) \doteq \frac{\partial \mathbf{r}_0(t)}{\partial p}. \tag{3}$$

The initial value problem associated with the partial derivative in Eq. (3) is referred to as the system of variational equations in this article, and is obtained by taking the partial derivative of Eq. (1). The result may be written as

$$\ddot{\mathbf{z}}_p = \mathbf{A}_0 \cdot \mathbf{z}_p + \mathbf{A}_1 \cdot \dot{\mathbf{z}}_p + \frac{\partial \mathbf{f}_1}{\partial p}, \tag{4}$$

where the 3×3 matrices $\mathbf{A}_0$ and $\mathbf{A}_1$ are defined by

$$A_{0[i,k]} = \frac{\partial f_i}{\partial r_{0,k}}; \quad A_{1[i,k]} = \frac{\partial f_i}{\partial \dot{r}_{0,k}}; \tag{5}$$

where f_i denotes the i-th component of the total acceleration $\mathbf{f}$ in Eq. (1). For $p \in \{a, e, i, \Omega, \omega, T_0\}$ Eq. (4) is a linear, homogeneous, second-order differential equation system with initial values $\mathbf{z}_p(t_0) \neq \mathbf{0}$ and $\dot{\mathbf{z}}_p(t_0) \neq \mathbf{0}$, whereas for $p \in \{q_1, \ldots, q_d\}$ Eq. (4) is inhomogeneous with zero initial values. Note that in the latter case, the homogeneous part of Eq. (4) is the same as for the parameters p defining the initial values.

The solutions of the variational equations related to the orbit parameters p_i, obtained either by numerical integration techniques (e.g., Beutler 2004) or by elaborate linear combinations as outlined in the next section, allow the eventual solution for corrections to the a priori orbit parameters p_{i0} in

a standard least-squares adjustment process of GPS observations together with all other relevant parameters. Finally, the improved orbit may be obtained using Eq. (2).

3 Pseudo-stochastic orbit modeling

Pseudo-stochastic orbit modeling may be considered as a realization of the well-known reduced-dynamic technique (Wu et al. 1991), which makes use of both the geometric strength of the GPS observations and the fact that satellite trajectories are particular solutions of a deterministic equation of motion. The attribute "pseudo" distinguishes our method from stochastic orbit modeling where a satellite trajectory is a solution of a stochastic differential equation (e.g., Jazwinski 1970). Our technique, however, introduces additional parameters referred to as pseudo-stochastic to the deterministic equation of motion. The attribute "stochastic" is chosen because they are characterized both by a priori known statistical properties like an expectation value and an a priori weight w_{a_i} given by an a priori variance $\sigma_{a_i}^2$ with

$$w_{a_i} = \frac{\sigma_0^2}{\sigma_{a_i}^2}\,, \tag{6}$$

where σ_0 denotes the a priori root mean square (RMS) error of unit weight. The a priori weights w_{a_i} from Eq. (6) constrain the estimated parameters on request, preventing them from deviating too much from the expectation value. Constraining pseudo-stochastic parameters, as described by Eq. (6), affects the influence of the dynamic models on the estimated trajectories at the full frequency range.

In this article we study different pseudo-stochastic parametrizations which are appropriate to reach an optimal balance between the use of a priori information on dynamics and the compensation for such information due to model deficiencies.

3.1 Instantaneous velocity changes (pulses)

Beutler et al. (1994) introduced instantaneous velocity changes as empirical parameters to improve the orbit quality of the GPS satellites in the daily routine processing at the center for orbit determination in europe (CODE). The once-per-revolution estimation of pulses compensates for deficiencies in modeling solar radiation pressure, which turned out to be the limiting factor when modeling high altitude satellites (Beutler et al. 1994).

Such pulses are also attractive for reduced-dynamic LEO POD, mainly because a large number can be set up efficiently. Focusing on one pulse v_i at time t_i in the predetermined direction $\mathbf{e}(t_i)$, the contribution of $q_i = v_i$ in $\mathbf{f}_1$ in Eq. (1) may formally be written as $v_i \cdot \delta(t - t_i) \cdot \mathbf{e}(t)$, where $\delta(t)$ denotes Dirac's delta distribution. As q_i does not explicitly depend on the velocity, the corresponding variational equation reads as

$$\ddot{\mathbf{z}}_{v_i} = \mathbf{A}_0 \cdot \mathbf{z}_{v_i} + \delta(t - t_i) \cdot \mathbf{e}(t) \tag{7}$$

with zero initial values. Equation (7) may be solved efficiently, since $\mathbf{z}_{v_i}$ may be written as a linear combination of the partial derivatives of the a priori orbit with respect to the six parameters defining the six initial conditions at t_0 (Beutler et al. 1994). A drawback, however, resides in the fact that $\dot{\mathbf{r}}(t)$ of the improved orbit is discontinuous at the epochs t_i.

3.2 Piecewise constant accelerations

Piecewise constant accelerations may be introduced for reduced-dynamic LEO POD to overcome the disadvantages of pulses (e.g., Jäggi et al. 2004a; van den IJssel and Visser 2005). In close analogy to the case of pulses, a large number of piecewise constant accelerations can be set up efficiently. Focusing on one acceleration a_i acting in the predetermined direction $\mathbf{e}(t)$ for $t_{i-1} \le t < t_i$, the contribution of $q_i = a_i$ in $\mathbf{f}_1$ in Eq. (1) is of the form $a_i \cdot \mathbf{e}(t)$ in the designated time interval. As q_i does not explicitly depend on the velocity, the corresponding variational equation reads as

$$\ddot{\mathbf{z}}_{a_i} = \mathbf{A}_0 \cdot \mathbf{z}_{a_i} + \begin{cases} \mathbf{e}(t); & t_{i-1} \le t < t_i \\ \mathbf{0}; & \text{otherwise} \end{cases} \tag{8}$$

with zero initial values. It was shown by Jäggi et al. (2004a) that all inhomogeneous systems (8) may be solved efficiently by forming linear combinations of only a small set of numerically integrated partial derivatives. A drawback, however, resides in the fact that $\dot{\mathbf{r}}(t)$ of the improved orbit is not differentiable at the epochs t_i.

3.3 Piecewise linear accelerations

Let us now develop the mathematical background for a new, more refined LEO orbit parametrization: $m+1$ accelerations a_i in predetermined directions $\mathbf{e}(t)$ at predefined epochs t_i, $i = 0, \ldots, m$ shall define a continuous acceleration over the entire orbital arc consisting of m linear pieces between subsequent epochs t_i. For one particular interval $t_{i-1} \le t < t_i$ the acceleration $\mathbf{a}(t)$ in the inertial system is represented by

$$\mathbf{a}(t) = \frac{t - t_{i-1}}{t_i - t_{i-1}} \cdot a_i \cdot \mathbf{e}(t) + \frac{t_i - t}{t_i - t_{i-1}} \cdot a_{i-1} \cdot \mathbf{e}(t), \tag{9}$$

which imposes continuity at the interval boundaries t_i. In close analogy to Sect. 3.2, the corresponding variational equation for the parameter a_i reads as

$$\ddot{\mathbf{z}}_{a_i} = \mathbf{A}_0 \cdot \mathbf{z}_{a_i} + \begin{cases} \left(\frac{t - t_{i-1}}{T_{i,i-1}}\right) \cdot \mathbf{e}(t); & t_{i-1} \le t < t_i; \quad i > 0 \\ \left(\frac{t_{i+1} - t}{T_{i+1,i}}\right) \cdot \mathbf{e}(t); & t_i \le t < t_{i+1}; \quad i < m \\ \mathbf{0}; & \text{otherwise} \end{cases}, \tag{10}$$

where $T_{i,j} \doteq t_i - t_j$. Equation (10) is closely related to Eq. (8) with an additional term proportional to t occurring in the inhomogeneous part.

Let us assume that the functions $\mathbf{z}_j(t)$, $j = 1, \ldots, 6$ are the partial derivatives of the a priori orbit $\mathbf{r}_0(t)$ with respect

to the six parameters defining the initial conditions at t_0. As these six functions $\mathbf{z}_j(t)$ form one complete system of solutions of the homogeneous part of Eq. (10), the solution of the inhomogeneous system can be obtained by the method of variation of constants. Beutler (2004) showed that the solution and its first time derivative may be written as a function of the homogeneous solutions

$$\mathbf{z}_{a_i}{}^{(k)}(t) = \sum_{j=1}^{6} \alpha_{ij}(t) \cdot \mathbf{z}_j{}^{(k)}(t); \quad k = 0, 1, \tag{11}$$

where the coefficients $\alpha_{ij}(t)$ are functions of time t to be determined. In matrix notation, $\mathbf{Z}_{[1,\ldots,3;\,j]} = \mathbf{z}_j, \mathbf{Z}_{[4,\ldots,6;\,j]} = \dot{\mathbf{z}}_j$, $j = 1, \ldots, 6$ and $\mathbf{h}_i{}^T = (\mathbf{0}^T, \partial\mathbf{a}(t)^T/\partial a_i)$, their solution may be obtained by definite integrals

$$\boldsymbol{\alpha}_i(t) = \int_{t_0}^{t} \mathbf{Z}^{-1}(t')\mathbf{h}_i(t')\mathrm{d}t' = \int_{t_{i-1}}^{t_i^*} \mathbf{Z}^{-1}(t')\mathbf{h}_i(t')\mathrm{d}t', \tag{12}$$

where $\boldsymbol{\alpha}_i{}^T = (\alpha_{i1}, \ldots, \alpha_{i6})$ and

$$t_i^* = \begin{cases} t_{i-1}; & t < t_{i-1} \\ t; & t_{i-1} \le t < t_{i+1} \\ t_{i+1}; & t \ge t_{i+1} \end{cases}. \tag{13}$$

This implies that the solution $\mathbf{z}_{a_i}(t)$ for the parameter a_i reads as

$$\mathbf{z}_{a_i}{}^{(k)}(t) = \begin{cases} \mathbf{0}; & t < t_{i-1} \\ \sum_{j=1}^{6} \alpha_{ij}(t) \cdot \mathbf{z}_j{}^{(k)}(t); & t_{i-1} \le t < t_{i+1} \\ \sum_{j=1}^{6} \alpha_{ij}(t_{i+1}) \cdot \mathbf{z}_j{}^{(k)}(t); & t \ge t_{i+1} \end{cases}. \tag{14}$$

Note that $\mathbf{z}_{a_i}(t)$ is a twice (continuously) differentiable function of time for the entire arc. For the case $t \ge t_{i+1}$ the coefficients $\alpha_{ij}(t_{i+1})$ are constant in time.

3.3.1 Efficient solution for $t_{i-1} \le t < t_i$

Let us introduce two auxiliary problems and write the solution of Eq. (10) as a function of these auxiliary problems. The parameters underlying the auxiliary problems are a constant acceleration $\bar{a}$ in predetermined direction $\mathbf{e}(t)$ over the entire orbital arc and the slope $\bar{b}$ of a linearly changing acceleration in direction $\mathbf{e}(t)$ over the entire orbital arc. The two corresponding variational equations read for the entire arc as

$$\ddot{\mathbf{z}}_{\bar{a}} = \mathbf{A}_0 \cdot \mathbf{z}_{\bar{a}} + \mathbf{e}(t) \quad \text{and} \quad \ddot{\mathbf{z}}_{\bar{b}} = \mathbf{A}_0 \cdot \mathbf{z}_{\bar{b}} + t \cdot \mathbf{e}(t). \tag{15}$$

As the difference $\boldsymbol{\Delta}_i \doteq (\mathbf{z}_{\bar{b}} - t_{i-1} \cdot \mathbf{z}_{\bar{a}})/T_{i,i-1} - \mathbf{z}_{a_i}$ solves the homogeneous differential equation system $\ddot{\boldsymbol{\Delta}}_i = \mathbf{A}_0 \cdot \boldsymbol{\Delta}_i$ in the designated time interval, its solution can be written as a linear combination of the functions $\mathbf{z}_j(t)$, therefore

$$\mathbf{z}_{a_i}{}^{(k)}(t) = \frac{1}{T_{i,i-1}} \cdot \mathbf{z}_{\bar{b}}{}^{(k)}(t) - \frac{t_{i-1}}{T_{i,i-1}} \cdot \mathbf{z}_{\bar{a}}{}^{(k)}(t) - \sum_{j=1}^{6} \beta_{ij} \cdot \mathbf{z}_j{}^{(k)}(t); \quad k = 0, 1. \tag{16}$$

Evaluating Eq. (16) at time t_{i-1} and taking Eq. (14) into account, the coefficients β_{ij} may be obtained as a solution of the following linear system of algebraic equations:

$$\begin{aligned} \sum_{j=1}^{6} \beta_{ij} \cdot \mathbf{z}_j(t_{i-1}) &= \frac{1}{T_{i,i-1}} \cdot \mathbf{z}_{\bar{b}}(t_{i-1}) - \frac{t_{i-1}}{T_{i,i-1}} \cdot \mathbf{z}_{\bar{a}}(t_{i-1}) \\ \sum_{j=1}^{6} \beta_{ij} \cdot \dot{\mathbf{z}}_j(t_{i-1}) &= \frac{1}{T_{i,i-1}} \cdot \dot{\mathbf{z}}_{\bar{b}}(t_{i-1}) - \frac{t_{i-1}}{T_{i,i-1}} \cdot \dot{\mathbf{z}}_{\bar{a}}(t_{i-1}). \end{aligned} \tag{17}$$

As Eq. (17) forms a linear system of six scalar equations for the six unknowns β_{ij}, it is possible to write the partial derivative from Eq. (16) in the designated time interval as a linear combination of the partial derivatives with respect to the parameters $\bar{a}$, $\bar{b}$, and the six partial derivatives $\mathbf{z}_j(t)$.

3.3.2 Efficient solution for $t_i \le t < t_{i+1}$

The difference $\boldsymbol{\Delta}^*{}_i \doteq (t_{i+1} \cdot \mathbf{z}_{\bar{a}} - \mathbf{z}_{\bar{b}})/T_{i+1,i} - \mathbf{z}_{a_i}$ solves the homogeneous differential equation system $\ddot{\boldsymbol{\Delta}}^*{}_i = \mathbf{A}_0 \cdot \boldsymbol{\Delta}^*{}_i$ in the designated time interval. $\mathbf{z}_{a_i}$ can therefore be written as

$$\mathbf{z}_{a_i}{}^{(k)}(t) = \frac{t_{i+1}}{T_{i+1,i}} \cdot \mathbf{z}_{\bar{a}}{}^{(k)}(t) - \frac{1}{T_{i+1,i}} \cdot \mathbf{z}_{\bar{b}}{}^{(k)}(t) - \sum_{j=1}^{6} \beta_{ij}^* \cdot \mathbf{z}_j{}^{(k)}(t); \quad k = 0, 1. \tag{18}$$

Evaluating Eq. (18) at time t_i and taking Eq. (14) into account, leads to the following linear system of algebraic equations for the coefficients β_{ij}^*:

$$\begin{aligned} \sum_{j=1}^{6} \beta_{ij}^* \cdot \mathbf{z}_j(t_i) &= \frac{t_{i+1}}{T_{i+1,i}} \cdot \mathbf{z}_{\bar{a}}(t_i) - \frac{1}{T_{i+1,i}} \cdot \mathbf{z}_{\bar{b}}(t_i) - \mathbf{z}_{a_i}(t_i) \\ \sum_{j=1}^{6} \beta_{ij}^* \cdot \dot{\mathbf{z}}_j(t_i) &= \frac{t_{i+1}}{T_{i+1,i}} \cdot \dot{\mathbf{z}}_{\bar{a}}(t_i) - \frac{1}{T_{i+1,i}} \cdot \dot{\mathbf{z}}_{\bar{b}}(t_i) - \dot{\mathbf{z}}_{a_i}(t_i). \end{aligned} \tag{19}$$

In analogy to the previous section, Eq. (19) forms a linear system of six scalar equations for the six unknowns β_{ij}^*. Again, the partial derivative from Eq. (18) may be written as a linear combination of the partial derivatives with respect to the parameters $\bar{a}$, $\bar{b}$, and the six partial derivatives $\mathbf{z}_j(t)$.

3.3.3 Efficient solution for $t \ge t_{i+1}$

Equation (14) implies that $\mathbf{z}_{a_i}^{(k)}(t_{i+1})$ may be computed by evaluating Eq. (18) at time t_{i+1}. The coefficients $\alpha_{ij}(t_{i+1})$ in Eq. (14) may therefore be obtained as a solution of the following linear system of algebraic equations:

$$\begin{aligned} \sum_{j=1}^{6} \alpha_{ij}(t_{i+1}) \cdot \mathbf{z}_j(t_{i+1}) &= \mathbf{z}_{a_i}(t_{i+1}) \\ \sum_{j=1}^{6} \alpha_{ij}(t_{i+1}) \cdot \dot{\mathbf{z}}_j(t_{i+1}) &= \dot{\mathbf{z}}_{a_i}(t_{i+1}). \end{aligned} \tag{20}$$

The method thus allows the set up of continuous piecewise linear accelerations with only one more parameter compared to the case of piecewise constant accelerations. An alternative formulation with offsets and drifts per interval would be less satisfying because of parameter doubling, and the necessity to put constraints at the interval boundaries when asking for continuity.

3.4 Summary

It was shown in the previous sections that a small set of numerically integrated partial derivatives is sufficient for all types of pseudo-stochastic parameters to solve all inhomogeneous variational equations, i.e., Eqs. (7), (8), and (10), by simple linear combinations. This avoids an explicit numerical quadrature of Eq. (12) for all pseudo-stochastic parameters, which makes it very efficient to set up large numbers of pseudo-stochastic parameters. Other empirical parameters, e.g., coefficients of a truncated Fourier series of periodic accelerations, do not offer such a possibility, which implies that the problem can be reduced only to numerical quadrature as Eq. (12) still holds. As more efficient methods are available to solve integrals than differential equations (Beutler 2004), numerically efficient solutions must be used in those cases.

4 Validation of CHAMP orbit results

The GPS final orbits and the 30 s high-rate satellite clock corrections (Bock et al. 2002) from the CODE analysis center were used together with the gravity field model EIGEN-2 (Reigber et al. 2003) and attitude data from the star tracker on board of CHAMP provided by GeoForschungsZentrum (GFZ) Potsdam to process undifferenced CHAMP GPS phase tracking data covering a time period from day 060/2002 to 260/2002. A development version 5.0 of the Bernese GPS Software (Hugentobler et al. 2001) was used to estimate the different orbit parameters mentioned in Sect. 3 together with all other relevant parameters like receiver clock corrections and real-valued carrier-phase ambiguities. The pseudo-stochastic parameters were set up in the radial, along-track and cross-track directions in the satellite co-rotating system with a time resolution of 6 min, which was found to be long enough to derive profit from the filtering effect of reduced-dynamic trajectories, and short enough to guarantee that different orbit parametrizations only induce short-periodic intra-interval differences in the orbit positions. In order to constrain pseudo-stochastic parameters "optimally", we followed the baseline described in (Jäggi et al. 2004b), where formal RMS errors of orbital positions (see Sect. 6.2) were found to be a good indicator for the actual orbit quality. Therefore, the pseudo-stochastic parameters were constrained according to Sect. 3 such that formal position errors are minimized.

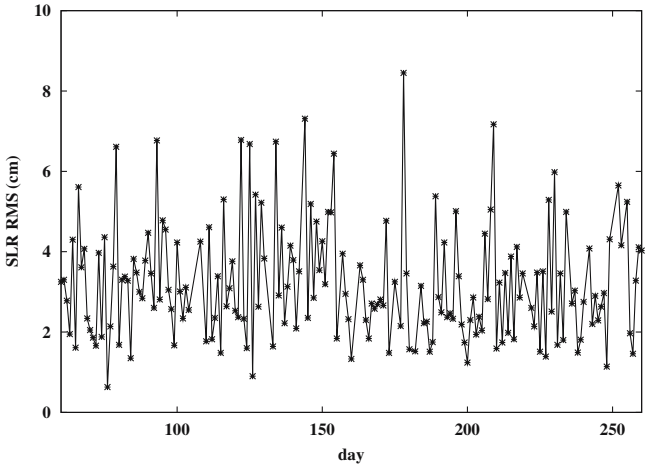

Fig. 1 SLR RMS (3.2 cm mean RMS) for days 060/2002 to 260/2002 obtained for reduced-dynamic CHAMP orbits. Almost no orbit differences exist between different parametrizations (see Fig. 9)

4.1 Orbit validation with SLR data

We used independent SLR measurements, which did not contribute to the orbit determination process, to compare the computed ranges between CHAMP and the SLR ground stations with the observed ranges for the 200 days mentioned. Figure 1 shows the daily RMS of SLR residuals obtained for the reduced-dynamic CHAMP 1-day orbital arcs based on a total of 21 SLR stations. Residuals larger than 0.3 m were considered as outliers and removed from the comparison, which reduced the amount of available data by about 3%. The mean SLR RMS of 3.2 cm without any significant offset indicates that the orbits are, in general, well represented by pseudo-stochastic parameters with a time resolution of 6 min. The result is in good agreement with the 3.0 cm found earlier for orbits computed for the time period of the CHAMP orbit comparison campaign (Boomkamp 2003), for which the most recent submissions from different analysis centers are listed in Table 1 (H. Boomkamp, private communication), which also includes estimates of the absolute orbit errors. Orbital arcs of significantly lower quality were found for the 200-day period as well, but these are often attributed to days with poor tracking conditions, e.g., dominated by large data gaps. Unfortunately, the residuals are too large and their number too small to distinguish subtle differences (see Fig. 9) between the various orbit parametrizations on the range level; they mainly reflect common systematic errors, e.g., sub-optimal data selections in the pre-processing procedures.

Table 1 SLR RMS and estimates of absolute orbit errors for days 140/2001 to 150/2001 of the CHAMP orbit comparison campaign

Institution	SLR RMS (cm)	Orbit RMS (cm)	Date of submission
AIUB	3.0	5.5	Feb. 2004
CSR	3.1	5.7	Jan. 2002
DEOS	3.6	6.5	Jun 2002
TUM	3.7	6.7	Feb. 2003
GRGS	4.0	7.2	Sep. 2002
GFZ	4.6	8.4	Sep. 2002

Note that old solutions might not have fully exploited the GPS data

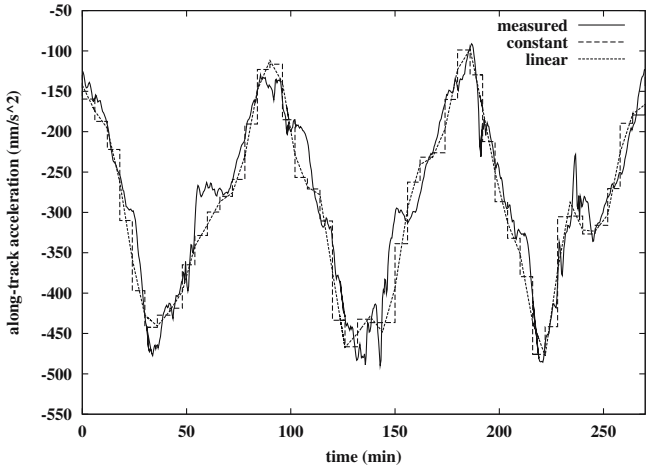

Fig. 2 Along-track comparison for day 198/2002 (1–5.5 h) between STAR accelerometer measurements (bias and scale removed) and estimated accelerations using the gravity field model EIGEN-2

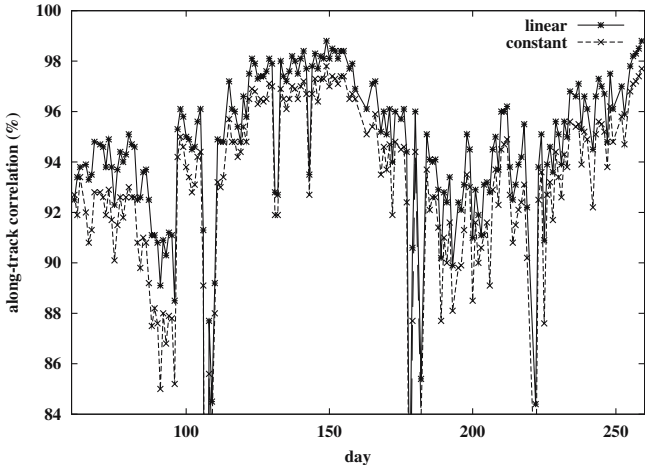

Fig. 3 Along-track correlation coefficients for days 060/2002 to 260/2002 between accelerometer data and estimated accelerations using the gravity field model EIGEN-2

4.2 Orbit validation with accelerometer data

Accelerometer data allow for a continuous verification of the estimated pseudo-stochastic accelerations (e.g., van den IJssel and Visser 2005; Jäggi et al. 2005). If POD is performed with a "perfect" gravity field model without models for the non-gravitational forces, pseudo-stochastic accelerations have to compensate "only" for the unmodeled accelerations acting on the satellite and may be directly compared with the accelerometer data.

Figure 2 shows, for a specific time interval of about three orbital revolutions, how piecewise constant and piecewise linear accelerations in the along-track direction agree with the measured accelerations (bias and scale provided by GFZ are removed) from the STAR accelerometer (Touboul et al. 1999), when the gravity field model EIGEN-2 is used. Apart from the well reproduced once-per-revolution signature, caused mainly by atmospheric drag, additional structures are occasionally tracked by the estimated accelerations, e.g., the large anomaly at 230 min during a North pole passage. Despite a generally high correlation of 93.9 and 95.1% for piecewise constant and piecewise linear accelerations, respectively, some obvious disagreements may be recognized, e.g., around 60 min. We noticed that small variations need not be necessarily tracked, because the large number of parameters still guarantees a good orbit representation due to the strong correlations between successive accelerations.

Figure 3 shows for both acceleration models the daily correlation coefficients between the estimated and the measured accelerations for the 200 days mentioned. The correlations indicate that along-track accelerations are, in general, well represented by pseudo-stochastic parameters with a time resolution of 6 min, but they also reveal noticeable variations over time. We observe, e.g., a reduced quality and stability of the comparison results around days 100/2002 and 200/2002. In particular for the second period of instability, we also noticed a considerable impact on cross-track comparisons (not shown), where the correlations dropped from a normal level of about 82 to only 39%. We suspect, however, that this effect is rather related to the accelerometer data than to orbit quality as no evidence for such a pattern was found in our SLR analysis. Moreover, cross-track accelerometer data show for this particular period, which begins after an orbit manoeuvre completed at day 163/2002, an increased sensitivity on the application of the Lorentz-correction provided with the level-2 accelerometer data.

Figure 3 shows that the correlation differences between both models are very stable at almost the same level of about 1.6%, which is only a small improvement for the piecewise linear model due to the chosen interval length of only 6 min. A similar level, although less stable, can also be observed in the cross-track direction. More pronounced effects for both directions could be expected for longer intervals, e.g., for 15 min with differences increasing up to about 8%, which is slightly larger than the effect (4.2%) to be expected from a pure once-per-revolution signal.

For more detailed comparisons and for the assessment of a statistically correct combination of very precise accelerometer data with GPS tracking data for reduced-dynamic POD based on piecewise constant accelerations, we refer to Jäggi et al. (2005). In that article, "overestimation" effects of a few percent due to the piecewise constant acceleration model were recognized to be relevant when combining both measurement types. If not taken into account, such effects affect accelerometer calibration parameters and orbit parameters in the combination.

5 Interpretation of pseudo-stochastic parameters

Pseudo-stochastic parameters reduce the influence of force field deficiencies only to a certain extent due to so-called discretization effects, which depend on the type and spacing of pseudo-stochastic parameters. We used simulated reduced-

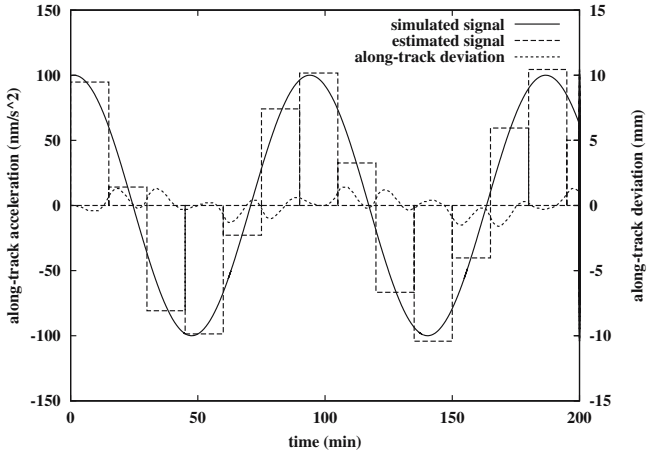

Fig. 4 Piecewise constant accelerations over 15 min compensate for an unmodeled along-track signal. The *dotted curve* denotes deviations with respect to the true orbit (simulated data)

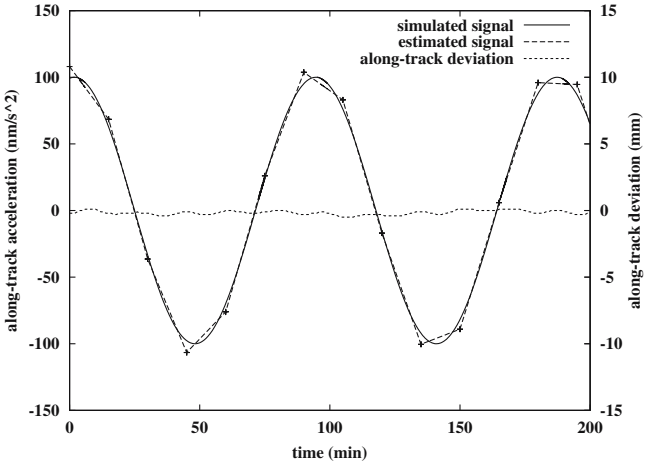

Fig. 5 Continuous piecewise linear accelerations over 15 min compensate for an unmodeled along-track signal. The *dotted curve* denotes deviations with respect to the true orbit (simulated data)

dynamic orbits to assess the importance of discretization effects for further orbit analysis based on re-parametrizations, e.g., for the determination of Earth's gravity field coefficients from reduced-dynamic LEO orbital arcs.

In the following section we assume that a deficient force field may be described by an analytic function $s \cdot f(t) \cdot \mathbf{e}(t)$ in direction $\mathbf{e}(t)$ with an unknown scale factor s. Instead of determining s directly from the GPS data, we investigate the most simple method to reconstruct this function, i.e., to determine the scale factor s after having performed an orbit analysis based on pseudo-stochastic parameters. In Sect. 5.2 we eventually solve the same type of problem with a more refined method and comment its capability to cope with more complex reconstruction problems.

5.1 Interpretability of single acceleration estimates

In Sect. 4.2 use was made of the possibility of directly comparing estimated accelerations with measured accelerometer data. In this section, we use a simulated environment to study the interpretability of pseudo-stochastic parameters by comparing piecewise constant and piecewise linear accelerations with the true, pointwise accelerations. Based on that, we estimate the level at which both types of estimated accelerations can be directly related to the pointwise values of a once-per-revolution acceleration.

5.1.1 Simulation scenario

The physical and mathematical models of the real data processing were used to simulate undifferenced GPS phase observations for the CHAMP satellite. An orbit affected in addition by a purely artificial once-per-revolution along-track acceleration with an amplitude of 10^{-7} m/s^2 served as the true orbit to simulate the error-free GPS data. An orbit with identical initial values, but not affected by the artificial signal, served as the a priori orbit.

Figures 4 and 5 show, for a specific time interval of about two orbital revolutions, how unconstrained piecewise constant and continuous piecewise linear accelerations, both estimated over 15 min to provoke noticeable discrepancies (see Sect. 4.2), approximate the unmodeled signal. A systematic "overestimation" may be observed in Fig. 4 (best visible at the symmetrically covered maximum at 185 min), which complicates a "straightforward" interpretation even in the case of unconstrained piecewise constant accelerations. As expected, the approximation is much better for the piecewise linear model shown in Fig. 5.

The orbit quality, which is expected to be less affected, is also shown in Figs. 4 and 5. We note that the along-track deviations from the true orbit are in general below the 2-mm level, even for the model based on piecewise constant accelerations with a coarse resolution in time. The once-per-revolution and once-per-interval variations in Fig. 4 reflect the remaining deficiencies in the piecewise constant model for the chosen time resolution. Comparing Fig. 5 reveals that the orbit solution based on piecewise linear accelerations shows no deficiencies at the millimeter level. The estimation of only one more parameter thus results in a considerable relative improvement with respect to Fig. 4. On an absolute scale, however, the gain is rather small.

5.1.2 Approximative method

One might try to estimate the amplitude s of the function $f(t) \cdot \mathbf{e}(t)$ from the previously estimated piecewise constant accelerations a_i, pointing into the direction $\mathbf{e}(t)$, in a new parameter estimation problem with the one and only parameter s. The corresponding pseudo-observation equations would simply read as

$$\frac{\partial a_i}{\partial s} \cdot s - a_i = v_i; \quad i = 1, \ldots, m \tag{21}$$

with v_i being the residuals of this new parameter estimation

problem. In view of approximating the function $s \cdot f(t)$ piecewise with Taylor series of degree zero, the partial derivative would intuitively be written as

$$\frac{\partial a_i}{\partial s} \doteq f(t_{m_i}) \quad \text{with} \quad t_{m_i} \doteq \frac{1}{2}(t_{i-1} + t_i) \; . \tag{22}$$

Alternatively, one might perform the parameter transformation defined by Eq. (21) already in the original POD process. Such a procedure would be very attractive because a direct calculation, i.e., numerical integration, of the partial derivative $\mathbf{z}_s(t)$ of the a priori orbit $\mathbf{r}_0(t)$ with respect to the parameter s would be unnecessary. Instead, $\mathbf{z}_s(t)$ could be computed as a function of the partial derivatives $\mathbf{z}_{a_i}$ with respect to the accelerations a_i as

$$\mathbf{z}_s(t) = \sum_{i=1}^{m} \mathbf{z}_{a_i}(t) \cdot \frac{\partial a_i}{\partial s} \; , \tag{23}$$

where the partial derivative of the acceleration a_i with respect to s would be approximated according to Eq. (22).

An amplitude estimation with Eqs. (21), or alternatively with Eq. (23), leads to the observed "overestimation" of the signal by about 4% for piecewise constant accelerations (when using piecewise linear accelerations one still encounters a systematic effect of 0.07%). The reason for this behavior is that the partial derivatives computed according to Eq. (22) are correct only up to terms of order zero in the length of the subintervals. This implies that the attempt to relate the parameters a_i directly to the pointwise accelerations introduces comparably large model errors, which may be acceptable for certain tasks in practice, e.g., for a combination based on piecewise linear accelerations, but certainly not for the most demanding tasks. Note that results from comparisons as shown in Sect. 4.2 are not that much affected if the partial derivatives are taken from the accelerometer data.

Figure 6 confirms these findings for the examples presented in this section. It shows the along-track deviations from the true orbit emerging from the original parameter estimation process (solid lines) and from the parameter estimation based on Eq. (22) (dotted lines). The results are given separately for the piecewise linear (top) and piecewise constant model (bottom). The bottom part clearly shows an unacceptable deterioration of the orbit quality due to a residual acceleration. The top part shows very similar orbits, which underlines that it is indeed possible to obtain acceptable results even with the approximative method.

5.2 Discretization errors

Figure 6 (bottom, solid line) shows that orbits of high quality may be obtained even when using piecewise constant accelerations with a modest time resolution. Obviously, the pure discretization errors due to pseudo-stochastic parameters must be much smaller than suggested by the "straightforward" interpretation from Sect. 5.1. In order to make correct use of the results achieved with pseudo-stochastic parametrizations, we have to go back to the original parametrization of the orbit determination problem.

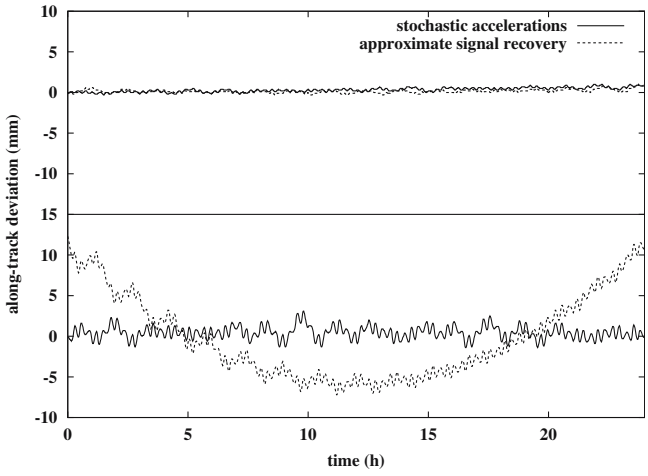

Fig. 6 Along-track deviations with respect to the true orbit (simulated data) due to piecewise linear accelerations (*top*) and due to piecewise constant accelerations (*bottom*) set up every 15 min

5.2.1 Reparametrization methods

Let us use a new set of $\tilde{n}$ orbit parameters denoted by $\{\tilde{p}_1, \tilde{p}_2, \ldots, \tilde{p}_{\tilde{n}}\}$. In order to simply re-parameterize the orbit determination after having performed the orbit determination with pseudo-stochastic parameters, i.e., based on the parameter set $\{p_1, p_2, \ldots, p_n\}$, we may use the orbital positions $\mathbf{r}(t_{m_i})$ established so far as pseudo-observations in a new orbit determination process. The observation equations of this new parameter estimation process read as

$$\sum_{k=1}^{\tilde{n}} \frac{\partial \mathbf{r}_0(t_{m_i})}{\partial \tilde{p}_k} \cdot (\tilde{p}_k - \tilde{p}_{k0}) - \delta\mathbf{r}(t_{m_i}) = \mathbf{v}_{\mathbf{r}i} \tag{24}$$

with

$$\delta\mathbf{r}(t_{m_i}) \doteq \sum_{l=1}^{n} \frac{\partial \mathbf{r}_0(t_{m_i})}{\partial p_l} \cdot (p_l - p_{l0}) \tag{25}$$

being the orbit improvements of the previously performed reduced-dynamic orbit determination and $\mathbf{v}_{\mathbf{r}i}$ the residuals of the new parameter estimation problem. Note that some parameters $\tilde{p}_k$ of the new orbit determination process may be identical to the reduced-dynamic orbit determination like, e.g., the Keplerian elements, whereas others are replaced. Typically, the pseudo-stochastic representation is substituted by a more physical representation accounting for force field deficiencies, e.g., a series of spherical harmonic coefficients representing the Earth's gravity field and scaling factors for non-conservative force models. Instead of using Eqs. (24) and (25) to re-parametrize the problem, it is also possible to use the first or the second time derivatives of these equations for the same purpose. The advantage of making use of the orbital dynamics by the initial conditions, however, is reduced.

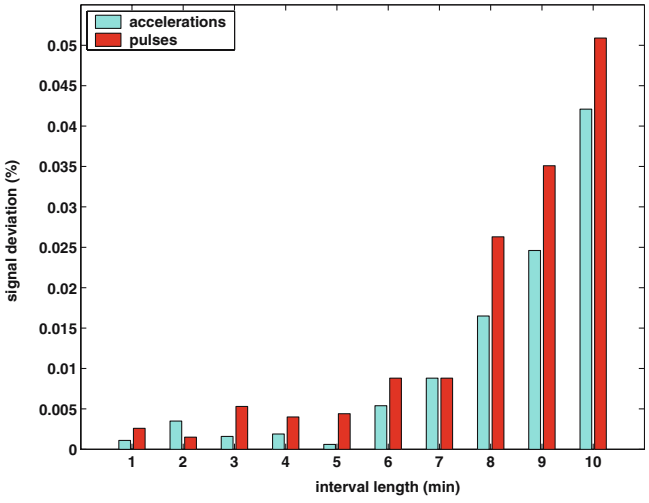

Fig. 7 Signal deviations (%) with respect to the true signal (simulated data) due to a recovery of the term $C_{6,3}$ with reduced-dynamic orbital positions

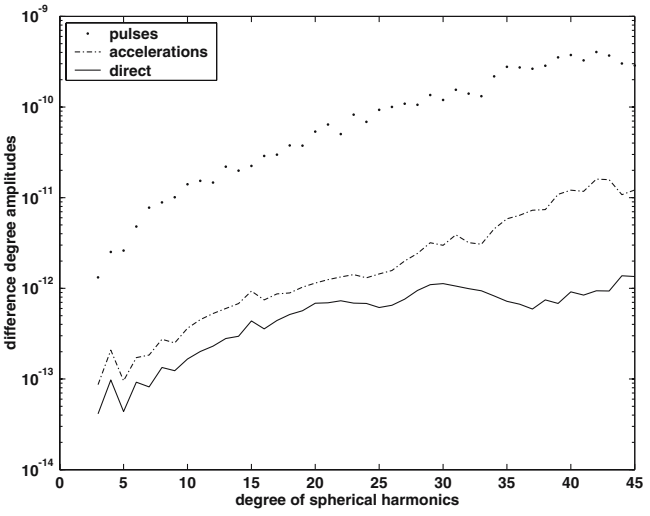

Fig. 8 Difference degree amplitudes with respect to the true gravity field model due to a direct recovery and due to recoveries with orbital positions based on 30 s pseudo-stochastic parameters

5.2.2 Approximative method

Starting with the second time derivative of Eq. (24), we can show which additional assumptions were implicitly made for the approximative method presented in Sect. 5.1.1 to estimate exactly one improvement s for the amplitude of the known function $f(t) \cdot \mathbf{e}(t)$. Equation (24) reads for this special case at time t_{m_i} as

$$\ddot{\mathbf{z}}_s \cdot s - \sum_{l=1}^{n} \ddot{\mathbf{z}}_{a_l} \cdot a_l = \mathbf{v}_i \ . \tag{26}$$

In order to obtain eventually Eq. (21), we replace the partial derivatives defined in Eq. (4) by the leading terms only, which read at time t_{m_i} as

$$\ddot{\mathbf{z}}_s \approx \frac{\partial \mathbf{f}_1}{\partial s}, \quad \ddot{\mathbf{z}}_{a_l} \approx \begin{cases} \frac{\partial \mathbf{f}_1}{\partial a_l}; & l = i \\ \mathbf{0}; & l \neq i \end{cases} , \tag{27}$$

where $\mathbf{f}_1(t_{m_i}) = a_i \cdot \mathbf{e}(t_{m_i})$. This finally leads to

$$\frac{\partial a_i}{\partial s} \cdot \mathbf{e}(t_{m_i}) \cdot s - a_i \cdot \mathbf{e}(t_{m_i}) = v_i \cdot \mathbf{e}(t_{m_i}) \ , \tag{28}$$

which is identical to Eq. (21), but formulated in the inertial system.

5.2.3 Simulation scenario

A new simulation study was performed to conduct two experiments based on the re-parametrization method proposed in Sect. 5.2.1. First, orbits based on unconstrained pseudo-stochastic parameters with different time resolutions were generated in an artificial a priori gravity field model with the geopotential term $C_{6,3}$ (arbitrarily selected) set to zero. In analogy to the simulation from Sect. 5.1.1, the pseudo-stochastic parameters have to compensate for an unmodeled signal of comparable amplitude, but with a main period of only one sixth of the orbital period. The derived orbital positions were subsequently used as pseudo-observations to recover the amplitude of the unmodeled signal according to Eqs. (24) and (25). Figure 7 shows the deviations of the recovered term $C_{6,3}$ with respect to its true value for different time resolutions of pulses and piecewise constant accelerations, which is a measure of the pure discretization error. In the situation comparable to the simulation from Sect. 5.1.1, i.e., with a resolution of 2.5 min, a deviation of only 0.002% is observed for piecewise constant accelerations. This implies that the signal amplitude can be recovered with a quality comparable to a direct estimation of the parameter, which is much better than for the approximate solutions from Sect. 5.1.2, at least in this simulation scenario. This indicates that orbits based on an appropriate spacing of pseudo-stochastic parameters, and therefore also the parameters themselves, preserve the information about the force field very well with a slightly better performance for the acceleration-based solutions than for the pulse-based solutions.

A second, more realistic experiment based on Eqs. (24) and (25) was conducted. Orbits based on pseudo-stochastic parameters with different time resolutions were generated in an artificial a priori gravity field with all geopotential terms set to zero with degrees larger than two. The derived orbital positions were subsequently used as pseudo-observations to recover the fully normalized coefficients of the true gravity field model (complete up to degree and order 45). Focusing again on the term $C_{6,3}$, we obtain much larger deviations in this second experiment, e.g., about 0.2% for accelerations with a resolution of 2 min. This effect, however, is rather caused by an aliasing effect of the higher order spherical harmonics than by discretization. Indeed, it is necessary to lower the parameter spacing at least down to 30 s to obtain a recovered gravity field from acceleration-based reduced-dynamic orbits which is competitive to a field obtained from a direct estimation. Figure 8 shows the difference degree amplitudes with respect to the true gravity field model for a 30 s acceleration-based solution.

Maximum coefficient deviations of about 8×10^{-12} (not shown) are reached only for some high degree zonal terms due to the almost polar CHAMP orbit. Figure 8 confirms that pseudo-stochastic parameters are able to preserve the information about the force field, if they are set up at an appropriate frequency (see remarks at the end of Sect. 6). The residual deviations shown in Fig. 8 are probably not significant because the ultimate limit for such a simulation due to numerical reasons is just about 10 times smaller, e.g., being the case for the direct estimation of the geopotential coefficients.

It is important to note that the quality of the recovered coefficients in this second experiment differs significantly for the different pseudo-stochastic orbit parametrizations. The use of pulse-based 30 s reduced-dynamic orbits, e.g., yields difference degree amplitudes which are more than 20 times higher than the difference degree amplitudes observed in Fig. 8 for the 30 s acceleration-based solution.

6 Differences due to the pseudo-stochastic orbit model

Let us now more closely inspect the differences between reduced-dynamic CHAMP orbits, derived from real GPS phase tracking data (day 198 of year 2002), for the different pseudo-stochastic orbit models presented in Sect. 3. The processing options are, unless otherwise stated, set to the values specified in Sect. 4.

6.1 Orbit differences

Figure 9 shows, for a specific time interval of 3 h, the along-track differences between the different reduced-dynamic orbits. The solid line shows the differences between the orbit generated with pseudo-stochastic pulses and the one generated with piecewise constant accelerations. The dotted line shows the differences between the orbit generated with piecewise linear accelerations and the one generated with piecewise constant accelerations. The very small differences illustrate that from the point of view of orbit modeling there is virtually no significant gain to be expected when using more refined orbit parametrizations with constraints, apart from the important fact that much lower time resolutions could be used. The along-track differences would still be below the half-centimeter level when halving the resolution of piecewise linear accelerations. The differences between the pulse and the acceleration solution in Fig. 9 must also be considered as small, although the effect of the instantaneous velocity changes with respect to accelerations can be observed well as sharp cusps at the pulse epochs every 6 min.

6.2 Formal orbit accuracies

More insight into the three orbit parametrizations is provided by analyzing the formal RMS errors of position and velocity, which may be obtained by applying the general law of error propagation on the full variance-covariance information. Figure 10 shows the formal position errors (3D) for the three pseudo-stochastic orbit models and confirms the almost identical orbit quality found in the previous subsection. Apart from the beginning and end of the orbital arc, the observed variations, e.g., the dominant once-per-revolution period, mainly reflect the tracking conditions (Jäggi et al. 2004b). The subtle differences between the different orbit parametrizations become obvious only in Fig. 11, a zoomed part of Fig. 10. Again, the sharp cusps from Fig. 9 are visible in the pulses solution, indicating a slightly lower orbit quality at the interval boundaries. It is interesting to note that piecewise constant accelerations show an opposite behavior with the lowest quality around the middle of the intervals as was already indicated by the simulation in Fig. 4. As expected, piecewise linear accelerations show the best performance over the entire arc with almost no intra-interval excursions.

The differences between the pseudo-stochastic orbit models become more pronounced at the velocity level. Figure 12 shows a zoomed view on the formal accuracies of the velocities (3D). Orbital velocities derived from the pulse solution show the expected discontinuities, whereas piecewise constant accelerations exhibit the same signatures that pulses showed at the position level. Thereby, the formal accuracies oscillate between the quality level of orbital velocities derived with pulses and orbital velocities derived with piecewise linear accelerations.

An improvement in LEO velocities due to the more refined parametrizations, e.g., pseudo-stochastic accelerations, could be of interest if reduced-dynamic orbits are used as pseudo-observations for gravity field recovery, e.g., by the energy balance approach, which is very sensitive to velocity errors (e.g., Gerlach et al. 2003). More important, however, is that the dynamics tends to be more reduced by acceleration parameters than by pulses, as mentioned in Sect. 5.2.3. To clarify this statement, we have to keep in mind that in the latter case the LEO trajectories correspond to the a priori gravity field model, except for the epochs where pulses are set up. Reduced-dynamic orbits based on accelerations, on the other hand, correspond rather to the actual gravity field during the entire arc as the unexplained gravity field signal is not only "concentrated" at the pulse epochs. This might eliminate to a certain extent (depending on the resolution of the accelerations and the applied a priori constraints, see Sect. 6.3) the dependency of a recovered gravity field from the a priori gravity field, which was reported by Gerlach et al. (2003), when probing the energy balance approach with reduced-dynamic orbits based on pulses. The use of reduced-dynamic orbits would make any cumbersome derivation of velocities obsolete and thus remove one of the problems associated with the pure kinematic approach (Földváry et al. 2004).

6.3 Impact of the a priori force field

Reduced-dynamic orbits always depend to a certain extent on the underlying dynamic model of the a priori orbit. The com-

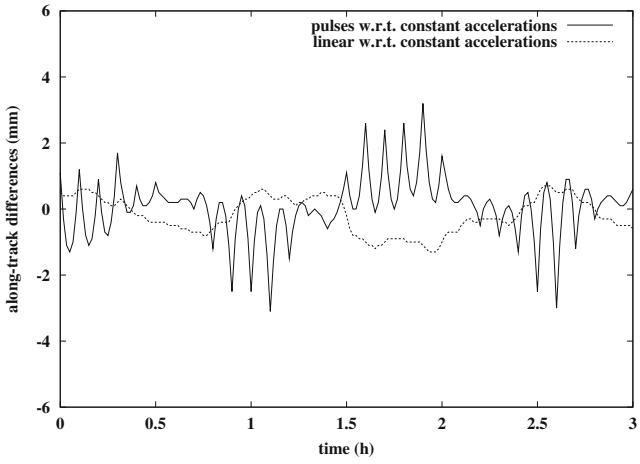

Fig. 9 Along-track orbit differences for day 198/2002 between an orbit based on piecewise constant accelerations and orbits based on pulses and piecewise linear accelerations, respectively

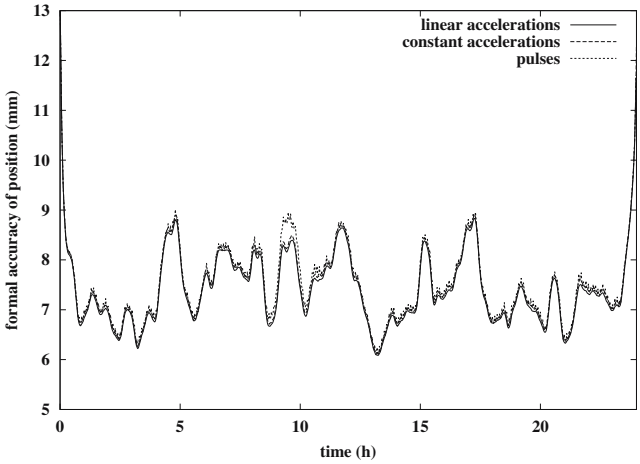

Fig. 10 Formal accuracies of orbital positions (3D) based on pulses, piecewise constant, and piecewise linear accelerations for day 198/2002

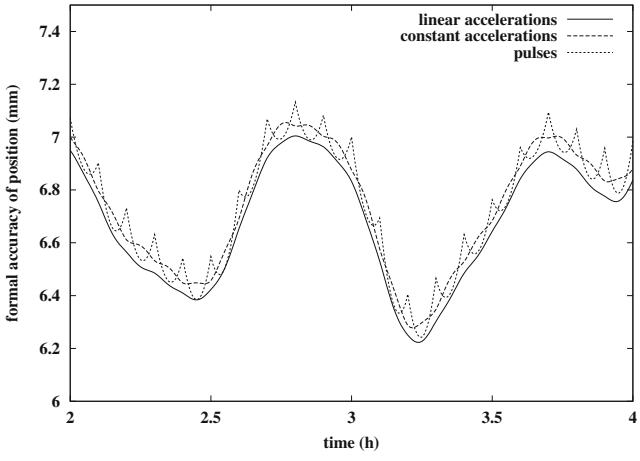

Fig. 11 Zoomed view of Fig. 10. Note the opposite behavior between pulses and piecewise constant accelerations at the interval boundaries

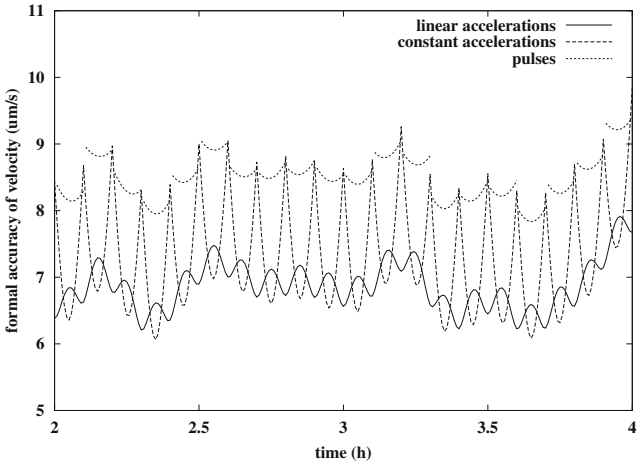

Fig. 12 Zoomed view of the formal accuracies of orbital velocities (3D) for day 198/2002. Piecewise constant accelerations behave like pulses on this level of differentiation

parison between identically parametrized reduced-dynamic orbits, which are estimated in different force fields, gives an impression of the (differential) influence of the a priori force models on the orbit. To illustrate this effect, two different ocean tide models, the CSR ocean tide model from Schwiderski (CSR 1995) and the CSR 3.0 global ocean tide model (Eanes and Bettadpur 1995), slightly differing in the low spherical harmonics up to degree 6, are used to demonstrate the capability of different orbit parametrizations to reduce the dynamic laws.

First, the same settings for the two almost identical reduced-dynamic orbits based on pulses and piecewise constant accelerations from Fig. 9 were used to compute the orbits in the two a priori force fields differing only by the above mentioned ocean tide models. The differences between the two pulse-orbits and the two orbits based on piecewise constant accelerations are shown in Fig. 13. We recognize that pseudo-stochastic orbit parameters considerably reduce the impact of the model change from several centimeters for a dynamic orbit (not shown) to a few millimeters, but there is virtually no difference between both parametrizations. Neither pulses, nor accelerations are able to fully absorb the effect due to the applied constraints. This implies an almost equal dependency of the estimated trajectories from the a priori force field, even in the very low frequency range below degree 6, because the applied constraints attenuate the signal absorption by pseudo-stochastic parameters at the full frequency range.

Figure 14 shows an analogue comparison for unconstrained pseudo-stochastic parameters with a time resolution of 6 (top) and 15 min (bottom), respectively. In the first case pseudo-stochastic parameters almost completely reduce the impact of the model change. It can be recognized that accelerations absorb the impact of the changed model slightly

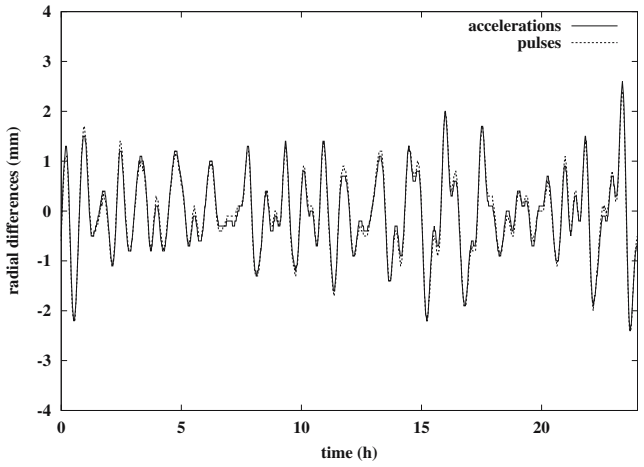

Fig. 13 Radial differences between identically parametrized orbits (constrained stochastic parameters every 6 min) computed in different a priori force fields. Almost no differences exist between different types of stochastic parameters

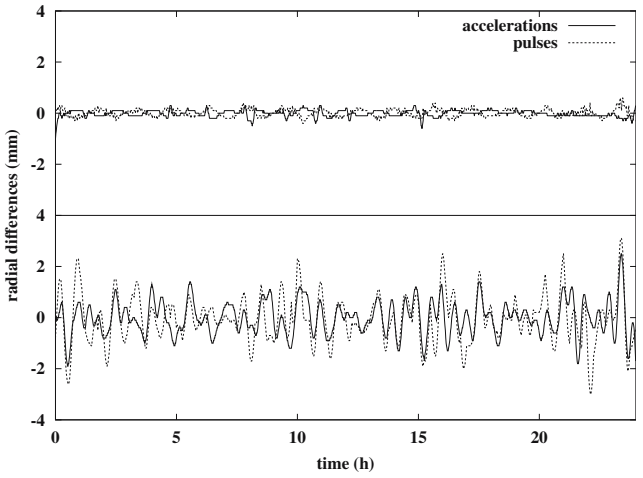

Fig. 14 Radial differences between identically parametrized orbits [unconstrained stochastic parameters every 6 (*top*) and every 15 min (*bottom*)] computed in different a priori force fields. Accelerations reduce the impact of the force model slightly more

more than pulses. The difference, however, is very small and would become zero for pseudo-stochastic parameters set up with the maximum resolution possible. In the low resolution case (Fig. 14, bottom), the differences are well visible, and would be even more pronounced on the velocity level for all examples shown. However, Fig. 14 (bottom) also shows that neither pulses, nor accelerations with a 15-min resolution are able to fully absorb the impact of the changed model on the estimated trajectories, because the resolution of pseudo-stochastic parameters is only equal to, but not shorter than the highest frequency induced by the model change. It must be expected, therefore, that higher order terms of the a priori force field still considerably influence the estimated trajectories.

It might make sense to use reduced-dynamic trajectories as an interface to derive gravity field coefficients in a subsequent procedure, if it can be guaranteed that the impact of the a priori force field used for the reduced-dynamic POD is reduced enough in the frequency range of interest. Using pseudo-stochastic parameters, they would have to be set up much more frequently, e.g., close to the observation sampling rate, as illustrated in Sect. 5.2.3 and in this section. The capability to estimate and use pseudo-stochastic parameters at high-rates, however, remains to be carefully studied, especially to determine whether the corresponding orbits would be beneficial over kinematic orbits.

7 Conclusions

Pseudo-stochastic orbit modeling techniques are well suited to derive reduced-dynamic LEO trajectories of highest quality by means of GPS observations. Simple algorithms may be used to set up a large number of such parameters, which make pseudo-stochastic orbit modeling techniques efficient and flexible. Just one additional parameter for each coordinate component has to be estimated together with all other parameters if the pseudo-stochastic model is improved from instantaneous velocity changes (pulses) to piecewise constant accelerations and from piecewise constant to piecewise linear accelerations, respectively. Such refined parametrizations are preferable from the physical point of view because they avoid discontinuities and undifferentiabilities at the velocity level for piecewise constant and piecewise linear accelerations, respectively.

The reduced-dynamic orbit results presented for CHAMP show, in general, a good agreement with independent measurements from other techniques. The estimated trajectories are confirmed by the SLR data at a level of 3.2 cm RMS with no significant offset. Orbital arcs of significantly lower quality are found as well, but are often attributed to days with poor tracking conditions. The estimated accelerations emerging from our GPS analysis are confirmed by the STAR accelerometer data at a correlation level of about 95% in the along-track direction and of about 82% in the cross-track direction. A small, but constant improvement of 1.6% in terms of correlation was found for the more refined acceleration model, whereas more pronounced benefits can be expected for longer acceleration intervals.

A simulation study showed that estimated piecewise linear accelerations can be directly interpreted as pointwise accelerations at a level below 0.1% even for long intervals, whereas the piecewise constant model is limited to a level of a few percent. The level of the pure discretization error of pseudo-stochastic parametrizations, however, was found to be much smaller, which indicates that they preserve the information about the force field very well. A simulation study showed that it is possible to use orbital positions obtained from pseudo-stochastic orbit modeling to derive gravity field coefficients with a quality comparable to a direct estimation, if the pseudo-stochastic parameters are set up at a sufficiently high rate. It was also found that the

coefficients are significantly better determined if a more refined pseudo-stochastic orbit model was used for the previous reduced-dynamic POD step.

From the pure orbit modeling point of view, refined pseudo-stochastic models just allow it to derive orbits of good quality with a reduced number of parameters. The main benefit of using a more refined pseudo-stochastic orbit model consists of more meaningful orbital velocities and accelerations. This, and the fact that the impact of the a priori force field is more reduced by refined pseudo-stochastic parameters could make LEO reduced-dynamic orbits interesting for the task of gravity field recovery. We clearly confirmed, however, that the time resolution of such parameters and the (possible) a priori weights are a very crucial issue.

Our results indicate that it could be interesting to study highly-reduced-dynamic orbits with pseudo-stochastic parameters estimated at a rate equal or close to the sampling rate of GPS data. Such orbits could serve as an alternative to kinematic orbits in the context of gravity field determination. A "routine"-generation of such orbits, however, is demanding in terms of the computational resources. It is therefore necessary to not only have an efficient parameter set up, but also improved algorithms for the efficient computation of all the parameters. These associated problems have been solved meanwhile and will be addressed in another article in the near future.

Acknowledgements The authors are grateful to GFZ Potsdam and CDDIS for providing the data for this investigation. The financial support by the Swiss National Science Foundation is gratefully acknowledged. Finally, we would like to thank W. Featherstone, N. Sneeuw, P. Moore, and two anonymous reviewers for their constructive comments.

References

Bertiger WI, Bar-Sever YE, Christensen EJ, Davis ES, Guinn JR, Haines BJ, Ibanez-Meier RW, Jee JR, Lichten SM, Melbourne WG, Muellerschoen RJ, Munson TN, Vigue Y, Wu SC, Yunck TP, Schutz BE, Abusali PAM, Rim HJ, Watkins MM, Willis P (1994) GPS precise tracking of TOPEX/POSEIDON: results and implication. J Geophys Res 99(C12):24449–24464

Beutler G, Brockmann E, Gurtner W, Hugentobler U, Mervart L, Rothacher M (1994) Extended orbit modeling techniques at the CODE processing center of the international GPS service for geodynamics (IGS): theory and initial results. Manuscripta Geodetica 19:367–386

Beutler G (2004) Methods of celestial mechanics. Springer, Berlin Heidelberg New York

Bock H, Hugentobler U, Springer TA, Beutler G (2002) Efficient precise orbit determination of LEO satellites using GPS. Adv Space Res 30(2):295–300

Boomkamp H (2003) The CHAMP orbit comparison campaign. In: Reigber C, Lühr H, Schwintzer P (eds) First CHAMP mission results for gravity, magnetic and atmospheric studies. Springer, Berlin Heidelberg New York, pp 53–58

CSR ocean tide model from Schwiderski (1995) ftp://ftp.csr.utexas.edu/pub/tide/oldfiles/spharm_schwid+

Eanes RJ, Bettadpur SV (1995) The CSR 3.0 global ocean tide model. Technical Memorandum 95-06, Center for Space Research, University of Texas, Austin

European Space Agency ESA (1999) The Four Candidate Earth Explorer Core Missions: Gravity Field and Steady-State Ocean Circulation Mission. ESA SP-1233 (1)

Földváry L, Švehla D, Gerlach C, Wermuth M, Gruber T, Rummel R, Rothacher M, Frommknecht B, Peters T, Steigenberger P (2004) Gravity model TUM-2Sp based on the energy balance approach and kinematic CHAMP orbits. In: Reigber C, Lühr H, Schwintzer P, Wickert J (eds) Earth observation with CHAMP, results from three years in orbit. Springer, Berlin Heidelberg New York, pp 13–18

Fu L, Christensen EJ, Yamarone CA, Lefebvre M, Ménard Y, Dorrer M, Escudier P (1994) TOPEX/POSEIDON mission overview. J Geophys Res 99(C12):24369–24381

Gerlach C, Földváry L, Švehla D, Gruber T, Wermuth M, Sneeuw N, Frommknecht B, Oberndorfer H, Peters T, Rothacher M, Rummel R, Steigenberger P (2003) A CHAMP-only gravity field model from kinematic orbits using the energy integral. Geophys Res Lett 30(20):2037. DOI 10.1029/2003GL018025

Hugentobler U, Schaer S, Fridez P (2001) Bernese GPS Software Version 4.2. Documentation, Astronomical Institute University of Berne, Berne

van den IJssel J, Visser PNAM, Patiño Rodriguez E (2003) CHAMP precise orbit determination using GPS data. Adv Space Res 31(8):1889–1895

van den IJssel J, Visser PNAM (2005) Determination of non-conservative accelerations from GPS satellite-to-satellite tracking of CHAMP. Adv Space Res 36(3):418–423

Jäggi A, Beutler G, Hugentobler U (2004a) Efficient stochastic orbit modeling techniques using least squares estimators. In: Sansò F (ed) A window on the future of geodesy. Springer, Berlin Heidelberg New York, pp 175–180

Jäggi A, Bock H, Hugentobler U, Beutler G (2004b) Comparison of different stochastic orbit modeling techniques. In: Reigber C, Lühr H, Schwintzer P, Wickert J (eds) Earth observation with CHAMP, results from three years in orbit. Springer, Berlin Heidelberg New York, pp 89–94

Jäggi A, Beutler G, Hugentobler U (2005) Reduced-dynamic orbit determination and the use of accelerometer data. Adv Space Res 36(3):438–444

Jazwinski AH (1970) Stochastic processes and filtering theories. Academic, New York

König R, Michalak G, Neumayer KH, Schmidt R, Zhu SY, Meixner H, Reigber C (2004) Recent developments in CHAMP orbit determination at GFZ. In: Reigber C, Lühr H, Schwintzer P, Wickert J (eds) Earth observation with CHAMP, results from three years in orbit. Springer, Berlin Heidelberg New York, pp 65–70

Kursinski ER, Hajj GA, Schofield JT, Linfield RP, Hardy KR (1997) Observing Earth's atmosphere with radio occultation measurements using the Global Positioning System. J Geophys Res 102(D19):23429–23465

Mayer-Gürr T, Ilk KH, Eicker A, Feuchtinger M (2004) ITG-CHAMP01: a CHAMP gravity field model from short kinematical arcs of a one-year observation period. J Geod 78:462–480

O'Keefe JA (1957) An application of Jacobi's integral to the motion of an Earth satellite. Astron J 62(1252):265–266

Reigber C (1989) Gravity field recovery from satellite tracking data. In: Sansò F, Rummel R (eds) Theory of satellite geodesy and gravity field determination. Springer, Berlin Heidelberg New York, pp 197–234

Reigber C, Balmino G, Schwintzer P, Biancale R, Bode A, Lemoine JM, Koenig R, Loyer S, Neumayer H, Marty JC, Barthelmes F, Perosanz F, Zhu SY (2002) A high quality global gravity field model from CHAMP GPS tracking data and accelerometry (EIGEN-1S). Geophys Res Lett 29(14):37–1. DOI 10.1029/2002GL015064

Reigber C, Schwintzer P, Neumayer KH, Barthelmes F, König R, Förste C, Balmino G, Biancale R, Lemoine JM, Loyer S, Bruinsma S, Perosanz F, Fayard T (2003) The CHAMP-only Earth Gravity Field Model EIGEN-2. Adv Space Res 31(8):1883–1888

Reigber C, Jochmann H, Wünsch J, Petrovic S, Schwintzer P, Barthelmes F, Neumayer KH, König R, Förste C, Balmino G, Biancale R, Lemoine JM, Loyer S, Perosanz F (2004) Earth gravity field and seasonal variability from CHAMP. In: Reigber C, Lühr H, Schwintzer P, Wickert J (eds) Earth observation with CHAMP, results

from three years in orbit. Springer, Berlin Heidelberg New York, pp 89–94

Švehla D, Rothacher M (2002) Kinematic and reduced-dynamic precise orbit determination of low Earth orbiters. Adv Geosci 1:47–56

Švehla D, Rothacher M (2004) Kinematic precise orbit determination for gravity field determination. In: Sansò F (ed) A window on the future of geodesy. Springer, Berlin Heidelberg New York, pp 181–188

Touboul P, Willemenot E, Foulon B, Josselin V (1999) Accelerometers for CHAMP, GRACE and GOCE space missions: synergy and evolution. Boll Geof Teor Appl 40:321–327

Visser PNAM, van den IJssel J (2003a) Aiming at a 1-cm orbit for low Earth orbiters: reduced-dynamic and kinematic precise orbit determination. In: Beutler G, Rummel R, Drinkwater MR, von Steiger R (eds) Earth gravity field from space - from sensors to Earth sciences. Kluwer, Dordrecht, pp 27–36

Visser PNAM, Sneeuw N, Gerlach C (2003b) Energy integral method for gravity field determination from satellite orbit coordinates. J Geod 77:207–216

Wu SC, Yunck TP, Thornton CL (1991) Reduced-dynamic technique for precise orbit determination of low Earth satellites. J Guid Control Dyn 14(1):24–30